Experimental investigation of the oxidative ageing mechanisms in bitumen

Pipintakos, Georgios; Vincent Ching, H. Y.; Soenen, Hilde; Sjövall, Peter; Mühlich, Uwe; Van Doorslaer, Sabine; Varveri, Aikaterini; Van den bergh, Wim; Lu, Xiaohu

Important note
To cite this publication, please use the final published version (if applicable).
Please check the document version above.

Experimental investigation of the oxidative ageing mechanisms in bitumen

Georgios Pipintakos [a,*], H.Y. Vincent Ching [b], Hilde Soenen [c], Peter Sjövall [d], Uwe Mühlich [a], Sabine Van Doorslaer [b], Aikaterini Varveri [e], Wim Van den bergh [a] and Xiaohu Lu [f]

[a] University of Antwerp, EMIB research group, Groenenborgerlaan 171, Antwerp 2020, Belgium

[b] University of Antwerp, Bimef research group, Universiteitsplein 1, Wilrijk 2610, Belgium

[c] Nynas NV, Groenenborgerlaan 171, Antwerp 2020, Belgium

[d] RISE Research Institutes of Sweden, 4P.O. Box 857, SE-501 15 Borås, Sweden

[e] Delft University of Technology, Pavement Engineering, Stevinweg 1, Delft 2628 CN, Netherlands

[f] Nynas AB, Raffinaderivägen 21, Nynäshamn SE 149 82, Sweden

* Corresponding author : georgios.pipintakos@uantwerpen.be

1 **Abstract**
2
3 Oxidative ageing in bituminous materials is considered one of the most important factors for distress types in road
4 applications. This paper aims to offer insights into the validity of commonly held beliefs regarding the oxidation
5 phases of ageing in bitumen, the fast- and the slow-rate phase, and explore the main oxidation products formed
6 upon ageing. In order to evaluate possible differences between bitumen types, the penetration grade as well as the
7 bitumen production process was varied. Thus, the ageing of three different binders was first studied by Fourier-
8 Transform Infrared (FTIR) and Electron Paramagnetic Resonance (EPR) spectroscopy. The formation of oxygen-
9 containing molecular structures on the bitumen surface during ageing was studied with Time-of-Flight Secondary
10 Ion Mass Spectrometry (TOF-SIMS). The results of FTIR reveal a gradual increase of sulfoxides upon ageing,
11 while the EPR results show an increase of organic carbon-centred radicals. In parallel, TOF-SIMS results provide
12 evidence for an increase of oxygenated compounds, such as SO_x^--, HO_x^-- and NO_x^--containing compounds. It
13 appears also that paramagnetic metal species, such as vanadyl-porphyrins, are insusceptible during ageing. Overall,
14 the findings of this study are in agreement with a mechanism comprising two rate-determining phases and support
15 the formation of different oxygenated products. It is believed that the experimental approach used in this work may
16 contribute further to an improved understanding of the ageing mechanisms in bitumen.

17 **Highlights:**

18 • EPR provides evidence for carbon-centred radical formation during exposure of bitumen to oxygen.

19 • TOF-SIMS demonstrates an increase of SO_x^--, HO_x^--, NO_x^--organics because of ageing.

20 • A fast- and a slow-rate phase for ageing can be distinguished with FTIR.

21 • EPR also shows that vanadyl-porphyrin species remain unchanged during ageing.

22 **Keywords:** bitumen; ageing mechanisms; EPR; FTIR; TOF-SIMS

2

1. Introduction

Bituminous binders are composed of a variety of organic molecules consisting of about 85% carbon, 10% hydrogen, heteroatoms such as nitrogen (0-2%), oxygen (0-2%), sulfur (0-9%) and traces of metals such as vanadium, iron and nickel [1,2]. Among the myriad of chemical functional groups of neat bitumen are the hydroxyl groups of phenols, imino groups of pyrrolic compounds, as well as carbonyl groups of ketones, carboxylic acids and 2-quinolones [3,4]. The heteroatoms in bituminous organic molecules not only modulate the polarity but also constitute chemical functional groups that can react and change. In particular, a wide variety of sulfur-containing compounds occurs preferentially within bituminous binders, such as sulfides, disulfides, sulfoxides, ring compounds (thiophenes, benzothiophenes and dibenzothiophenes) and their alkyl derivatives [5].

Previous studies have demonstrated the significance of bitumen chemistry as it can assist in the unravelling of the oxidative ageing mechanisms in bitumen [6]. More specifically, ageing of bitumen is a process of autoxidation as the binder reacts with oxygen, generating new compounds that may continue to react with oxygen. To date, a number of studies support that during the ageing process, the active functionalities of bitumen molecules are decomposed through the oxidative dehydrogenation of polycyclic perhydroaromatics generating intermediate hydroperoxides [7,8]. Through the years, different mechanisms have been proposed to describe this phenomenon ranging from an oxycyclic reaction mechanism [9] up to a dual sequential binder oxidation mechanism [4,10]. According to the latter, two major oxidation routes may exist, namely the chemically distinct "fast-spurt" and "slow/long-term" routes [6,10–12]. This idea has gained considerable support since a direct link with the asphalt production stages can be established [13].

Among other factors, it should be acknowledged that the temperature may vary between different asphalt mixture applications (hot, warm, cold) or stages of the service life. Thus, certain standardised ageing protocols exist in order to simulate the different stages. It has been reported previously that the temperature during the short-term ageing in production stage has a stronger effect on the intensity of oxygenated products than the temperature during the long-term ageing in service life [14,15]. Moreover, the literature emphasises that an increase of 10 ºC may double the reaction rate and a relatively high temperature may destroy certain microstructures of the polar species [6]. Care should be taken when reviewing these mechanisms by taking into account the corresponding thermal history varying per asphalt application. Nevertheless, the ageing mechanisms will remain somewhat similar independently of the thermal history and they may be affected only in terms of quantity of products and reaction rate.

The studies presented so far provide evidence that the ageing-produced ketones and carboxylic acids are of high polarity, generating strong associations, expressed through their Van der Waals forces. Subsequently, the polar compounds of bitumen may interact with each other [16]. Possible chemical changes could induce stronger interactions and change the bitumen microstructure which may have implications in the mechanical behaviour. Given this, there is a growing body of evidence that an increase in apparent molecular weight due to increased molecular interactions can reduce the mobility of molecules to flow which, in turn, will influence the bitumen rheology [17–20]. Eventually, there is a widespread recognition that the severity of ageing can be tracked by capturing the change in certain functional groups [13,18,19,21,22].

It appears that experimental validation of the underlying mechanisms has been confined primarily to sulfoxide and carbonyl formation. Considerable research has been devoted to the determination of these functional groups via chemical analysis such as Fourier-Transform Infrared spectroscopy (FTIR) [14,21,22]. When it comes to the fractions of bitumen, previous studies were also limited to the explanation that a sequential reaction, of aromatic to resin and finally to asphaltene fraction, takes place [23–25]. No further evidence for the mechanisms behind these changes and the accompanied reasoning has been provided apart from microstructural changes observed with the use of microscopy [26–29]. Challenges arise when specific products of ageing in bitumen are needed to be confirmed experimentally.

This study addresses a number of questions regarding the ageing mechanisms of bitumen. An important issue is the validation of the previously proposed oxidation schemes. This was achieved by utilising a number of spectroscopic techniques. In particular, support was provided by FTIR, EPR and TOF-SIMS spectroscopy. Links

71 between the results of the three techniques under predefined oxidation time and temperature, finally, review certain
72 hypotheses for the ageing mechanisms of bitumen.

73 **2. Materials and methods**

74 *2.1. Materials and ageing treatment*

75 Three bituminous binders were used as specified in Table 1, namely, a hard binder A and two soft binders B and
76 C. Binders A and B originate from a wax-free crude oil, and differ only in the degree of distillation processing.
77 Binder C is a visbroken residue, containing natural wax (crystallisable compounds) and coming from a different
78 crude oil.

79 Table 1: Properties of the bituminous binders

Material	Property		Binder		Test Method
Bitumen		A	B	C	
	Penetration 25 ºC (0.1 mm)	16	189	190	EN1426
	Softening point (ºC)	61.1	37.5	39.2	EN1427
	Penetration index, Ip	-1.06	-1.46	-0.63	EN12591
	Viscosity 135ºC (mm^2/s)	1285	203	N/D	EN12595

80 To simulate the oxidative ageing of the three binders, a modified thin film oven test (M-TFOT) was used: a
81 binder film of approximately 1 mm thick was aged in an oven at 50 °C, for the FTIR and the TOF-SIMS
82 measurements. That was not the case for the EPR measurements where binder films of thickness 3-5 mm were aged
83 directly in polypropylene tubes. All the analyses were performed without prior sample mixing as additional heating
84 may have a considerable effect on the oxidation process.
85 In all cases the film thickness was kept minimum in order to exclude, as much as possible, the diffusion effect
86 from the coupled reaction-diffusion phenomenon of ageing. By minimising the film it is assumed that the diffusion
87 effect will be eliminated and primarily oxidation will be the dominating process [30–32]. Instrumental constraints
88 resulted in thicker films for the EPR analyses which may have experienced an increased diffusion. It should be
89 noted that the EPR analyses measured the entire bitumen sample, therefore the number of spins derived from the
90 EPR spectra were divided by the exact mass of the sample in order to extract a fair comparison value independently
91 of the small fluctuation of thickness compared to FTIR and TOF-SIMS films.
92 All the ageing tests were conducted at 50 °C, as at this temperature a fast- and a slow-rate reaction can be clearly
93 differentiated. Additionally, at this low temperature the decomposition of sulfoxides can be eliminated [6]. For the
94 FTIR and EPR measurements, tests were conducted after several ageing time intervals, while for TOF-SIMS tests
95 were conducted at two ageing times; the starting point with ageing time zero and after 8 days. These ageing times
96 were derived from preliminary FTIR and EPR findings for a prolonged ageing time up to 56 days. A graphical
97 summary including the main outcomes for each technique is presented in Figure 1.

4
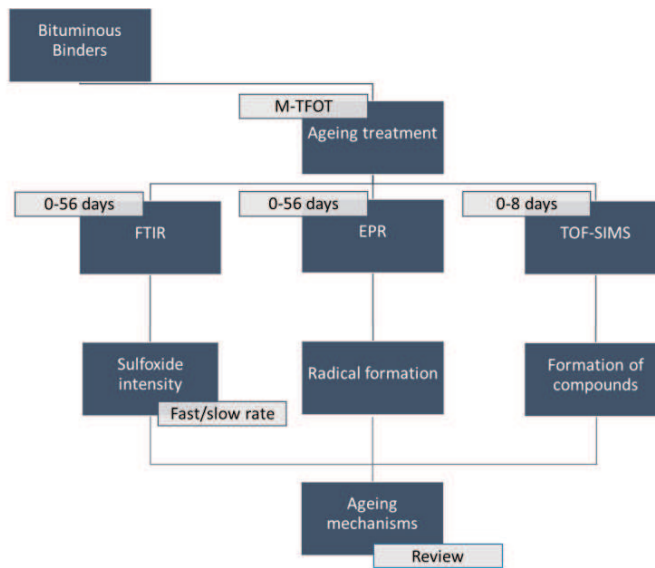
Figure 1: Flowchart of the experimental part and objectives

98

2.2. Spectroscopic techniques

99

2.2.1. Attenuated Total Reflectance-Fourier Transform Infrared (ATR-FTIR)

100
101
102   The FTIR analysis was performed with a Thermo Scientific Nicolet iS10 FTIR spectrometer equipped with an
103 Attenuated Total Reflectance (ATR) fixture and a Smart Orbit Sampling Accessory. At least three replicas were
104 measured per ageing time interval. The collected spectra were acquired with 32 repetitive scans and ranged from
105 400 cm^{-1} to 4000 cm^{-1} with a resolution of 4 cm^{-1}.
106   In this study, a widely accepted protocol for the determination of the normalised intensity of certain functional
107 groups was followed [21]. More specifically, the areas around certain peaks, as depicted for exemplary spectra of
108 bitumen A in Figure 2, were calculated. To do this, a baseline is introduced based on the limits of each band given
109 in Table 2 and the area that is enclosed is computed based on the trapezoidal rule that approximates a definite
110 integral. The focus here was exclusively on sulfoxides, which are more prone to be produced during oxidation at
111 lower temperatures, like the one used (50 ºC). For the quantification of the normalised ageing intensity of
112 sulfoxides, Equation 1 is applied. Despite the applied normalisation method, upon oxidation, discrepancies due to
113 changes in the refractive index and subsequently in the effective path length controlled by the depth of penetration
114 of the evanescent wave into the sample, may still arise. These effects, if present, are in the best scenario negligible.
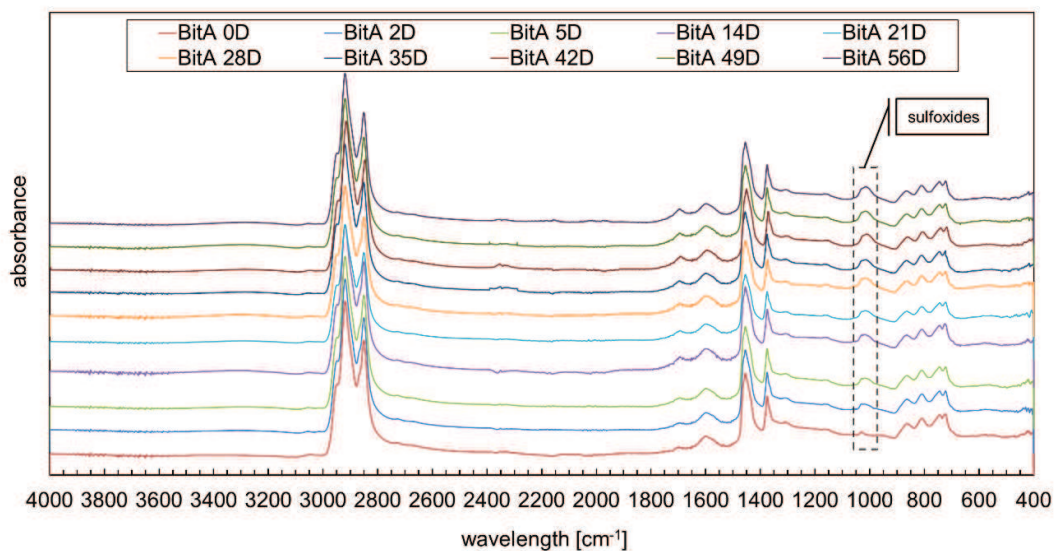
Figure 2: Evolution with ageing time (0-56 days) for exemplary FTIR spectra of bitumen A.

$$\text{Normalised sulfoxide intensity} = \frac{A_{1030}}{\sum_{n=1}^{N} A_n} \qquad (1)$$

Table 2: Band limits of the utilised FTIR functional groups

| Functional group	Bond vibration	Band limits for baseline (cm^{-1})	Area around peak n, (A_n)
Long Chains	(CH$_2$)$_n$ rock (n ≥ 4) bending	734-710	724
Aromatic structures	C=CH adjacent out of plane bending	783-734	743
Aromatic structures	C=CH adjacent out of plane bending	838-783	814
Aromatic structures	C=CH singlet out of plane bending	912-838	864
Sulfoxides	S=O stretching	1047-995	1030
Branched aliphatic structures	CH$_3$ symmetric bending	1390-1350	1376
Aliphatic structures	CH$_3$ asymmetric bending	1525-1395	1460
Aromatic structures	C=C stretching	1670-1535	1600
Carbonyls	C=O stretching	1753-1660	1700
Alkyl groups	C-H symmetric stretching	2880-2820	2862
Alkyl groups	C-H asymmetric stretching	2990-2880	2953

118   ## *2.2.2. Electron Paramagnetic Resonance (EPR)*

119   EPR is a spectroscopic technique able to identify paramagnetic centres and molecules in a material, i.e. the
120   components containing unpaired electrons. It is particularly useful to characterise organic radicals and transition-
121   metal ions. Therefore, continuous-wave (cw) EPR spectra of aged and unaged bitumen samples were recorded with
122   a Bruker Elexsys E680 spectrometer mounted with an ER 4102ST TE102 mode resonator working at ~9.75 GHz
123   (X-band). Polypropylene Eppendorf tubes were used as sample holders ensuring that the total material quantity did
124   not overfill the cavity. Preliminary measurements on the unaged binder A showed a two-component EPR spectrum
125   consisting of contributions of a vanadyl centre (VO^{2+}, $S = 1/2$) and an organic carbon-centred radical. The former
126   is characterised by an axial powder pattern with typical hyperfine splitting due to the interaction of the electron
127   with the ^{51}V nucleus ($I = 5/2$), and the latter gives rise to an unresolved single line close to the free electron value
128   ($g_e = 2.0023$) (Figure 3a). This was also the case for binder B and C. Power saturation measurements showing
129   different relaxation rates (Figure 3b) confirmed the presence of the two species. For all subsequent measurements,
130   0.5 mW was chosen, because this was close to the highest microwave power level before either species became
131   saturated (i.e. signal intensity vs √microwave power was linear, Figure 3b). Simulation of the experimental spectra
132   with Matlab2018b using the EasySpin-6.0 module [33], gave the EPR parameters of the two species (Table 3) as
133   well as the relative amounts of spins between the two ('weights').
134

135   Table 3: EPR parameters of the VO^{2+} and organic radical signal in binder A, B and C as determined by simulations of the room temperature
136   cw X-band EPR spectra of the binders.

Binder	VO^{2+}				Radical
	$g_\perp$	$g_\parallel$	$A_\perp$ /mHz	$A_\parallel$/mHz	g_{iso}
A	1.9831 ± 0.0002	1.9616 ± 0.0002	160.4 ± 0.4	472.0 ± 1.5	2.0025 ± 0.0002
B	1.9831 ± 0.0003	1.9620 ± 0.0002	160.2 ± 0.5	471.9 ± 1.3	2.0026 ± 0.0003
C	1.9832 ± 0.0005	1.9610 ± 0.0008	160.0 ± 0.4	475.6 ± 1.2	2.0027 ± 0.0002

137   The EPR parameters of the observed VO^{2+} centres are consistent with those of VO^{2+} porphyrin centres found in
138   heavy crude oils [34,35], while the parameter of the radical signal has been previously postulated to be carbon-
139   based [36]. For the ageing experiments, at least three replicas were measured per ageing interval with the centre
140   field at 341 mT, sweep width of 20 mT, resolution of 2048 points, modulation amplitude of 0.1 mT and modulation
141   frequency of 100 kHz over 2 scans. The number of spins in each sample was estimated by comparing the double
142   integral of each spectrum with those of TEMPO (2,2,6,6-tetramethyl-1-piperidinyloxyl, a chemical compound used
143   commonly as a structural probe for radicals' characterisation) in toluene solution standards. The number of VO^{2+}
144   or organic radical spins in each sample was estimated by comparing the weights used in the spectral simulations.
145   Division by the mass of the sample gave the number of spins per gram of sample given in Figure 5.
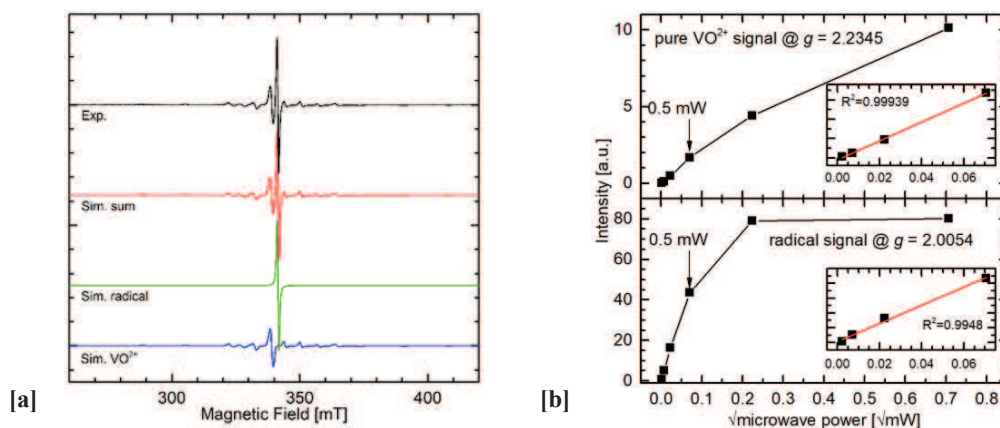
146   Figure 3: Room temperature cw X-band EPR spectra of binder A with its simulations [a] and its signal intensity contrasted with square root of
147   the power at different g-values, with insets showing a linear fit of selected powers [b].

2.2.3. Time-of-Flight Secondary Ion Mass Spectrometry (TOF-SIMS)

149   The analysis principle of TOF-SIMS includes the bombardment of the sample surface with high-energy primary
150   ions and analysis of the emitted (secondary) ions with respect to mass-to-charge ratio (m/z). The obtained mass
151   spectra provide molecular information about the sample surface and imaging of specific ions is accomplished by
152   scanning the primary ion beam over a selected analysis area and acquiring separate mass spectra in each pixel [37].
153   In principle, the selection of the number of pixels in the TOF-SIMS analyses, i.e. the number of data points within
154   the analysis area, is based on the fact that the pixel size should be matched with the diameter of the primary ion
155   beam.
156   Here, the TOF-SIMS analyses were conducted in a TOF-SIMS IV instrument (IONTOF GmbH, Germany)
157   using 25 keV Bi_3^+ primary ions and low-energy electron flooding for charge compensation. The sample temperature
158   was kept at -80 °C during analysis to prevent diffusion/segregation in the bitumen due to the vacuum environment
159   of the TOF-SIMS instrument. Bitumen samples were deposited on silicon wafer substrates and subsequently
160   allowed to cool down according to a special protocol [2]. Positive and negative ion spectra were acquired over
161   analysis areas of 200 μm x 200 μm (128 x 128 pixels) or 500 μm x 500 μm (256 x 256 pixels) at three locations of
162   each sample, with the instrument optimised for high mass resolution (m/Δm ≈ 3000-6000). In the case of bitumen
163   C, additional positive and negative ion data was acquired (i.e. high resolution images) with the instrument optimised
164   for high image resolution (lateral resolution ≈ 0.5 μm).

165   **3. Results and discussion**

166   *3.1. Dual-oxidation route*

167   *3.1.1. FTIR analyses*

168   The results of FTIR analyses show a steep increase of the normalised sulfoxide intensity followed by a steady
169   milder increase for all three binders (Figure 4). Binders A and C were found to have almost completed the initial
170   rapid increase at about 5 days, whereas binder B reached this transition point at about 2 days. It becomes apparent
171   that at 8 days of controlled ageing the slow-rate oxidation reaction has been initiated for all the binders.
172   Given that sulfoxides are considered to be one of the end products of both a fast and a slow reaction [6], oxidation
173   kinetics were approximated in the following way for the product evolution. Assuming pseudo first-order kinetics

8

174 and that the rate of the slow reaction is rather small, the evolution of an end product P, of a dual-sequential oxidation
175 mechanism, can be described by Equation 2:

176
$$P(t) = P_{f\infty}(1 - e^{-k'_f t}) + P_{s\infty}k'_s t + C \qquad (2)$$

177 where $P(t)$ is the amount of product as function of time; $P_{f\infty}$ and $P_{s\infty}$ are amounts of product from the fast and
178 slow reactions, respectively at the reaction endpoint; k'_f and k'_s are pseudo first order rate constants of the fast and
179 slow reactions, respectively; and C is a constant [12]. The FTIR results for all three binders can be reasonably fitted
180 to Equation 2 with their parameters given in Table 4.

181 Table 4: Parameters used for fitting Equation 2 to the FTIR normalised sulfoxide intensity and their R^2.

Binder	$P_{f\infty}$ [$\times 10^{-3}$ a.u.]	k'_f [$\times 10^{-6}$ s^{-1}]	$P_{s\infty}k'_s$ [$\times 10^{-6}$ s^{-1}]	C [$\times 10^{-3}$ a.u.]	R^2
A	8.5 ± 0.2	7.3 ± 2.2	1.33 ± 0.03	4.69 ± 0.08	0.9997
B	6.3 ± 0.1	13.8 ± 1.5	0.67 ± 0.04	4.14 ± 0.01	0.9998
C	7.9 ± 0.7	5.9 ± 1.2	1.00 ± 0.07	8.12 ± 0.65	0.9827

182 From this analysis, k'_f was determined to be fastest for binder B, followed by A then C. Moreover, the percentile
183 increase of the normalised sulfoxide intensity of the virgin binder up to the completion of the ageing treatment used
184 here, was evaluated. This percentile increase demonstrates that binder A suffered from a harsher oxidation effect
185 (317.88%) followed by binder B (224.52 %) and C (148.39 %), under the same ageing conditions.
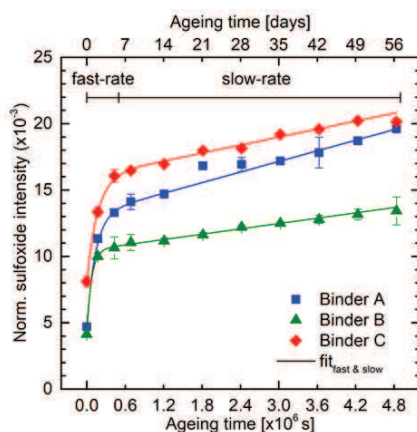

186 Figure 4: Evolution of the FTIR normalised sulfoxide intensity over ageing time and the fitting used, based on a dual-sequential model [4,12].

187   Semi-quantitative methods to analyse the FTIR spectrum can be useful for identifying and characterising the
188 evolution of specific oxidation products. Consistent with previous studies, this work demonstrated an initial rapid
189 increase of sulfoxides followed by a slow-rate formation [4,6]. Hence, the kinetics of the normalised sulfoxide
190 intensity can establish a simple way to distinguish different oxidation rates. At least, they can give a rough
191 estimation for the two phases under the given ageing conditions.

192 ***3.1.2. EPR analyses***

193   The time-dependent evolution of the EPR spectra of the three binders was investigated in the same timeframe
194   as with the FTIR, up to 56 days. The graphs in Figure 5a and 5b respectively, show the evolution of the organic
195   carbon-centred radicals and VO^{2+} species over ageing time. Interestingly, in all cases the amount of VO^{2+} spins
196   remained relatively constant as the samples were aged (a zeroth order line can be fitted with the error bars), while
197   an increase was observed for the organic carbon-centred radicals (Figure 5a). A comparison of the binders used in
198   this study indicates also that the relative increase of organic carbon-centred radicals in binder C was about 1.5-2
199   times higher in comparison with binders A and B.

200
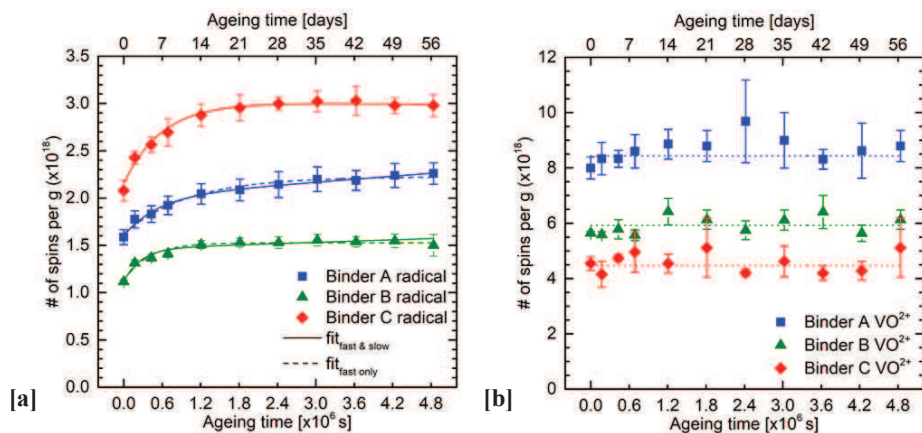
201   Figure 5: Evolution of the carbon-centred radical and the used fitting, based on a dual-sequential or a fast reaction model [a] and VO^{2+} centres
202   over ageing time [b].

203   Although the results for the evolution of the carbon-centred radical EPR signal could also be fitted using
204   Equation 2 (parameters given in Table 5), for each binder the contribution from the slow reaction term was almost
205   negligible and for binder C it was even negative, which is contrary to a dual fast and slow production of end
206   products model. These carbon-centred radicals are believed to be only produced and also subsequently consumed
207   during the slow-rate phase. Since they are observable, their rate of production must be faster than their rate of
208   consumption. In all cases, the evolution of the carbon-centred radical EPR signal is dominated by a mono-
209   exponential component which strongly suggests that their rate of production is kinetically controlled by the fast-
210   rate phase. This means that the previously reported oxygen-centred free radicals, assumed to be generated in the
211   fast-rate phase [4], are able to immediately abstract protons attached to benzyl rings to yield carbon-centred
212   radicals. In contrast, since the subsequent consumption of these carbon-centred radicals appear to be much slower,
213   it must be governed by the overall kinetics of the slow-rate phase. Once the system enters the slow-rate phase, the
214   rate of oxygen-centred free radical production and thus carbon-centred radical production will become comparable
215   to their rate of consumption, and therefore, as can be seen in Figure 5a, no net increase in the amount of carbon-
216   centred radicals is observed.
217   In line with these hypotheses, the k_f' values obtained for the radical production were within a similar range to
218   those for sulfoxide production. Similarly, the k_f' for binder B was again the fastest, which suggests that both organic
219   carbon-centred radicals and sulfoxide productions in the fast reaction may be controlled by the same rate-limiting
220   process.

221   Table 5: Parameters used for fitting the EPR spin counting of the radical signal and their R^2.

| Binder	Reaction(s)	$P_{f\infty}$ [×10¹⁷ spins g⁻¹]	k_f' [×10⁻⁶ s⁻¹]	$P_{s\infty}k_s'$ [×10¹⁰ spins g⁻¹s⁻¹]	C [×10¹⁷ spins g⁻¹]	R^2
A	Fast & slow	4.1 ± 0.5	1.9 ± 0.4	5.2 ± 1.4	16.0 ± 0.2	0.9862
	Fast only	6.1 ± 0.3	1.0 ± 0.1	N/A	16.0 ± 0.2	0.9772
B	Fast & slow	3.4 ± 0.4	3.7 ± 0.9	2.2 ± 1.4	11.0 ± 0.2	0.9710
	Fast only	4.0 ± 0.2	2.6 ± 0.4	N/A	11.0 ± 0.2	0.9695
C	Fast & slow	8.7 ± 0.9	1.7 ± 0.3	-0.73 ± 0.02	21.0 ± 0.4	0.9771
	Fast only	8.5 ± 0.4	1.8 ± 0.2	N/A	21.0 ± 0.4	0.9797

222   It is interesting to mention that, in contrast to FTIR results, the harsher oxidation effect was observed for binder
223   C. This difference can be explained by the fact that binder C was the result of a visbreaking process, which is a
224   mild cracking process, resulting in radical formation. This can explain the higher initial organic carbon-centred
225   radical concentration observed in bitumen C (Figure 5a).
226   In addition, the VO²⁺ signal appears to stay constant over the ageing time in Figure 5b, for the three investigated
227   binders. It can be exploited as an indicator of the vanadium content in petroleum [38]. Of particular interest is that
228   this assignment seems to remain unaffected by ageing and could be potentially used as a marker for the origin of
229   the bitumen.
230   Together the two spectroscopic techniques give strong evidence for the two rates of a dual-oxidation route. It is
231   important to mention when comparing the two different spectroscopic techniques that efforts to lessen the effect of
232   different film thickness were taken into account. Given this, FTIR supports that between 2 and 5 days for all the
233   examined binders the fast-rate reaction has finished, whereas EPR proves that carbon-centred radicals, which is
234   believed to be produced and subsequently consumed during the slow-rate phase, actually evolve with the fast-rate
235   phase kinetics. The ageing time interval of 8 days was used afterwards for TOF-SIMS surface analyses to unravel
236   the main products after the combined effects of the fast- and slow-rate phase.

237   ### 3.2. Oxygenated products

238   TOF-SIMS was used to analyse molecular changes on the bitumen surfaces upon ageing. Positive and negative
239   ion spectra were acquired for the three binders (A, B and C) in the unaged state and after 8 days of ageing, at which
240   point the fast-rate phase is mainly completed and the slow-rate phase has been initiated. Representative spectra of
241   the unaged and aged samples of bitumen A and C are presented in Figure 6 and ion assignments of peaks relevant
242   to ageing are listed in Tables 6 and 7. No clear changes due to ageing can be observed in the major peaks of the
243   spectra, indicating that the effect of ageing on the molecular surface structure is relatively small. In contrast, clear
244   differences can be observed between the spectra of bitumen A and C, mainly reflecting the wax content of bitumen
245   C. As reported previously wax segregates effectively in bitumen to form a thin layer of wax, largely covering the
246   surface, which can be observed in the spectra of bitumen C [28]. The higher intensities of peaks in bitumen C
247   represent aliphatic species, whereas the spectrum of the wax-free bitumen A displays higher intensities of peaks
248   representing aromatic species, as well as N- and S-containing organics.
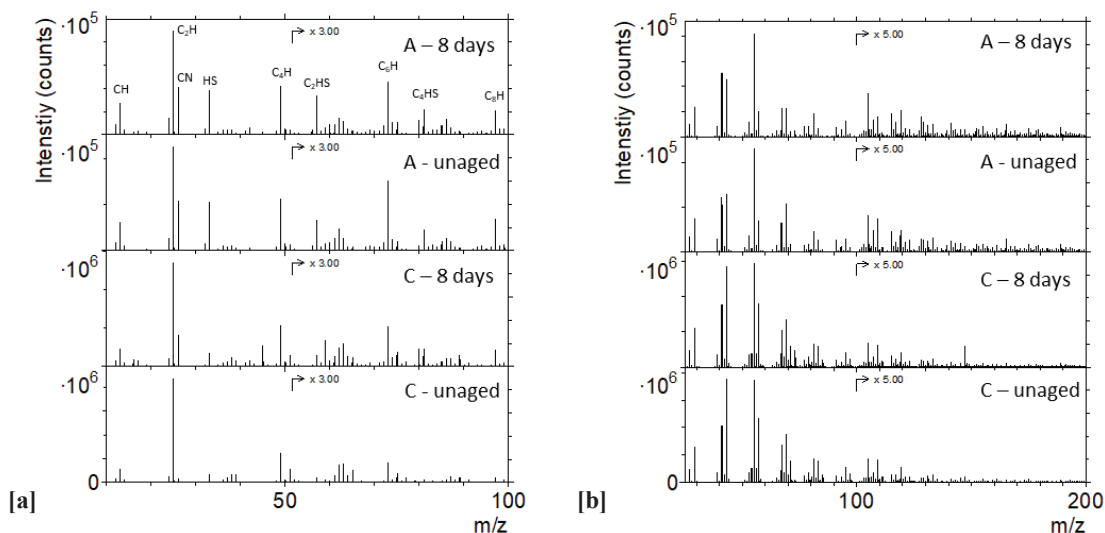
249   Figure 6: Negative [a] and positive [b] ion spectra of bitumen A and C before and after M-TFOT ageing for 8 days.

250   Although the major peaks in the TOF-SIMS spectra are essentially unchanged, the effect of ageing can be
251   observed by consideration of oxygen-containing fragment ions, including SO_x-, NO_x- and O_x-containing organic
252   ions, which are present at lower signal intensities, mainly in the negative ion spectra (see Tables 6-7).

253   Table 6: Utilised oxygenated peaks for negative ions of TOF-SIMS.   Table 7: Utilised oxygenated peaks for positive ions of TOF-SIMS.

Ion	Observed mass (m/z)	Assignment of molecular structure
O^-	15.994	O_x-containing
$OH-$	17.004	HO_x-containing
CN^-	26.003	N-containing
$C_3H_2^-$	38.016	Aliphatic
$C_3H_3^-$	39.024	Aliphatic
C_2HO^-	41.006	HO_x-containing
CNO^-	42.002	NO_x-containing
CHO_2^-	45.001	HO_x-containing
$C_4H_3^-$	51.023	Aliphatic
CSO^-	59.967	SO_x-containing
SO_2^-	63.963	SO_x-containing
C_4HO^-	65.003	HO_x-containing
$C_5H_5^-$	65.038	Aliphatic
$C_2H_3SO^-$	74.989	SO_x-containing
$C_6H_5^-$	77.037	Aliphatic
SO_3^-	79.961	SO_x-containing
SO_4H^-	95.959	SO_x-containing
C_3NO^-	96.999	NO_x-containing

Ion	Observed mass (m/z)	Assignment of molecular structure
CH_3O^+	31.020	O_x-containing
$C_3H_5^+$	41.047	Aliphatic
$C_2H_3O^+$	43.020	O_x-containing
$C_3H_7^+$	43.066	Aliphatic
$C_4H_7^+$	55.068	Aliphatic
$C_4H_9^+$	57.087	Aliphatic
$C_3H_7O^+$	59.049	O_x-containing
$C_5H_7^+$	67.066	Aliphatic
$C_5H_9^+$	69.087	Aliphatic
$C_5H_{11}^+$	71.117	Aliphatic
$C_6H_9^+$	81.087	Aliphatic
$C_6H_{11}^+$	83.112	Aliphatic
$C_6H_{13}^+$	85.135	Aliphatic
$C_7H_{11}^+$	95.106	Aliphatic
$C_7H_{13}^+$	97.129	Aliphatic
$C_8H_{13}^+$	109.128	Aliphatic
$C_9H_7^+$	115.059	Aromatic
$C_9H_{11}^+$	119.105	Aliphatic
$C_{10}H_8^+$	128.068	Aromatic
$C_{13}H_9^+$	165.079	Aromatic

254 The oxygen-containing fragment ions of the three binders were analysed based on normalised signal intensities
255 and categorised into SO_x-containing (Figure 7a) and HO_x-containing fragments (Figure 7b). A strong increase in
256 the intensity of the fragments with the generic formula RSO_x and RHO_x can be observed, strongly indicating the
257 formation of sulfoxide- and oxygen-related compounds as a result of ageing. Additionally, for all binders the
258 amount of cyanate fragments, with generic formula RNO^-, also increased during oxidation. It is important to note
259 here that signal intensities of different ions should not be compared to indicate concentration differences between
260 the corresponding molecular species, as the yield of formation for different ions may vary considerably. Instead,
261 signal intensities of the same ion can be compared to indicate concentration differences between samples of the
262 specific species that it represents.
263 Comparing the different bitumens, the effect of ageing is generally higher for bitumen A compared to bitumen
264 B, but the strongest effect is observed for the wax-containing bitumen C. Furthermore, bitumen A and B show no
265 effect of ageing on the intensities of fragment ions without oxygen content, including CN^- and aliphatic/aromatic
266 hydrocarbon fragments. For bitumen C, however, ageing results in increased intensities of CN^- (Figure 8), as well
267 as in hydrocarbon fragments representing aromatic species, and decreased intensities of aliphatic hydrocarbon
268 fragment ions, see Figure 9.
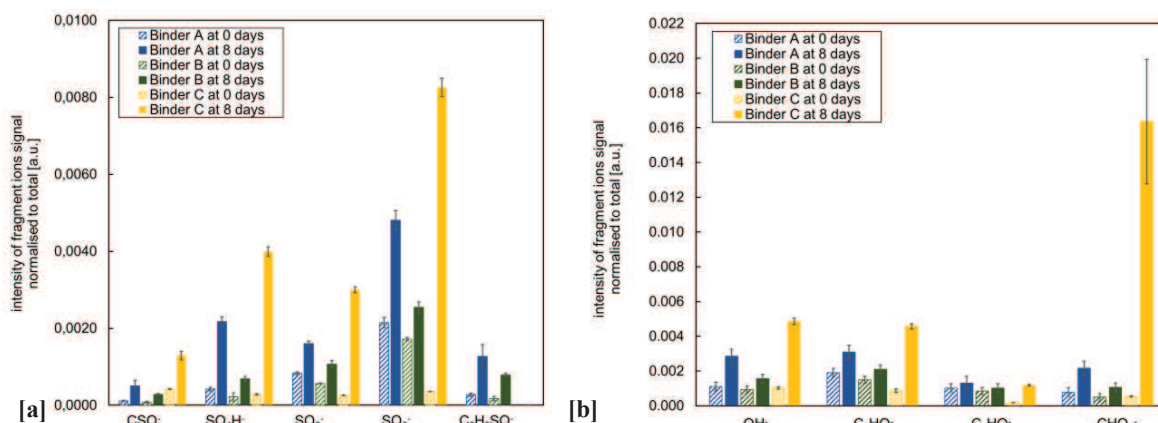
269 Figure 7: Intensity of SO_x-containing [a] and HO_x-containing compounds via TOF-SIMS for all three binders [b]. Mean values from three
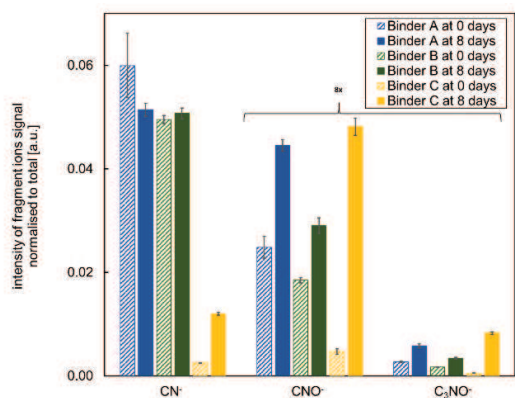270 measurements are presented and error bars are +/- 1 standard deviation.
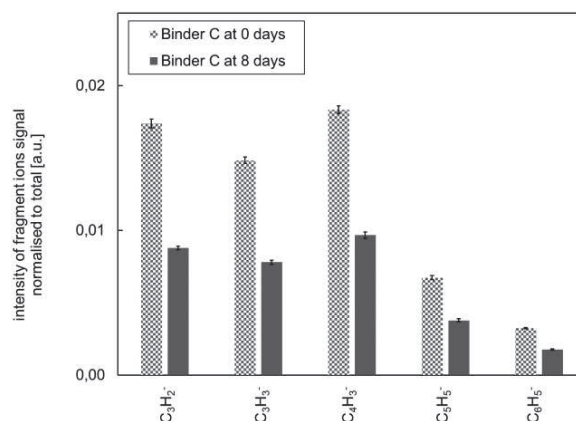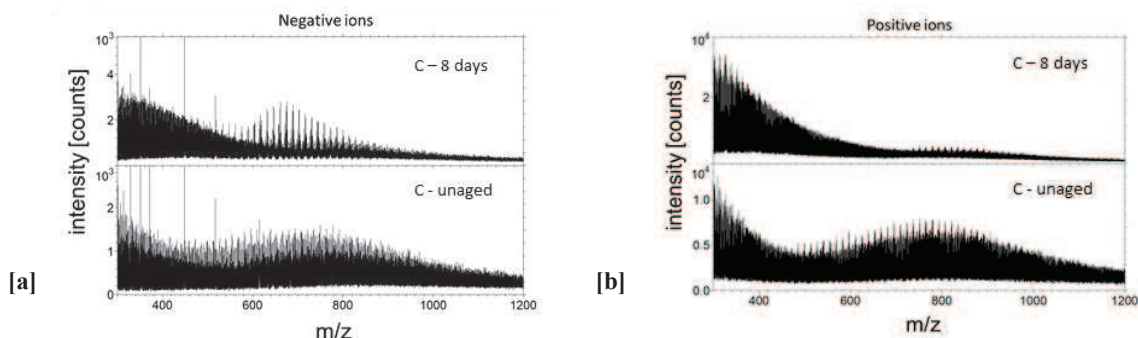

Figure 8: Intensity of nitrogen-containing compounds.

Figure 9: Negative ions of binder C assigned to aliphatic

Figure 10: High mass range of negative [a] and positive ion spectra of bitumen C before and after M-TFOT ageing for 8 days [b].

Next to sulfoxide formation during the slow reaction, alcohol groups may also be produced [4,39]. The sulfoxide intensity observed with FTIR has been assigned, up to now, completely to this functional group. However, an overlap with other HO_x-containing groups may exist in the corresponding infrared absorption band (around 1100 cm^{-1}), indicating that alcohols and sulfoxides may coincide. Whereas the origin of the increase of this infrared absorption band upon ageing, therefore, is unknown, the observed increase of HO_x-containing fragments with TOF-SIMS is consistent with the formation of alcohols and/or carboxylic acids. It can thus be speculated that ageing results in the formation of more polar species, e.g. alcohols or carboxylic acids, which then may affect the molecular interactions and eventually the rheology of bitumen.

Previously [40,41], it was found that nitrogen-containing compounds can be identified in oxidised bitumens without significantly changing upon ageing [6]. In this study, the increase of RNO^- fragments indicates that additional oxidation products, those of nitrogen-containing compounds are present upon ageing, which should be taken into account in a future oxidation scheme. It can also be expected that the concentration of the different heteroatoms may have an impact on the intensity of the different fragments.

In Figure 10, TOF-SIMS spectra of bitumen C are presented at a higher mass range, m/z 350-1200, where the peaks to a larger extent correspond to intact or nearly intact molecular species. The envelope of peaks at m/z 500-1000 in both negative and positive ion spectra can be assigned to intact wax molecules, as previously articulated by Lu [28], for which the intensity reduction upon ageing is consistent with the reduced intensities of the aliphatic fragment ions upon ageing (Figure 9). Interestingly, ageing of bitumen C produces a new envelope of peaks at m/z 600-800 in the negative ion spectrum. Although unambiguous identification of these peaks is not possible due to the limited mass resolution, a mass separation of m/z = 14 between equivalent peaks and the exact mass of the peaks is consistent with molecules comprised of nearly saturated aliphatic hydrocarbon chains with an added SO_x functional group. For example, a peak observed at m/z 689.63 is consistent with $C_{45}H_{85}SO_2$, containing both an aliphatic and a small aromatic structure in which the S=O may be included. The latter may be taken as a consequence of oxidation and its subsequent sulfoxide formation.

For the positive ions, the effect of ageing was mainly observable in binder C. A clear increase in the intensities of O-containing organic ions was observed, reflecting the formation of oxidation products on the bitumen surface (Figure 11). Furthermore, positive ions of aliphatic fragments show a decreasing trend as can be seen in Figure 11, in contrast to polycyclic aromatic hydrocarbons (PAH) which increase upon ageing (Figure 12), consistent with the observations for the negative ions (Figure 9).

14
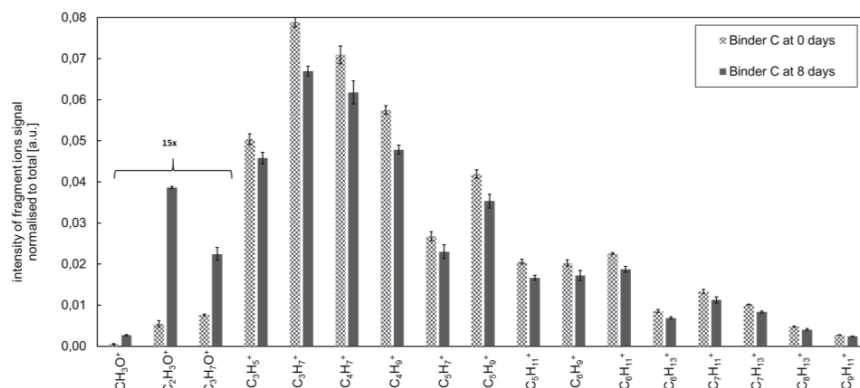
Figure 11: Intensity of O-containing and aliphatic fragments in selected positive ions.
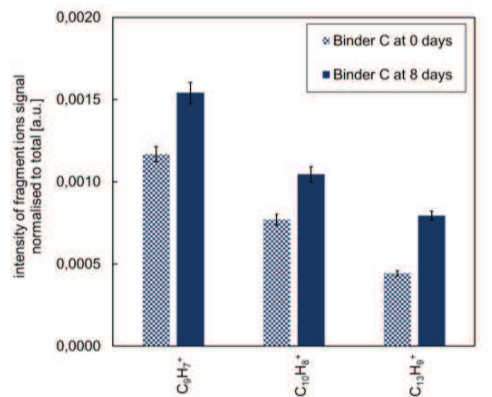
Figure 12: Intensity of PAH fragments in selected positive ions.

Finally, in order to investigate the spatial distribution of the wax fraction and the ageing-related molecular species on the surface of bitumen C, high-resolution TOF-SIMS images were generated (Figures 13). A clear phase separation with a governing aliphatic phase is observed, with particles about 5-10 μm in size which covered most of the surface. Apparent wax-related particles (represented by aliphatics) cover most part of the surface and the spaces between these particles display increased signal intensities of ageing-related ions, such as O^-. CN^- and $(H)SO_x^-$ (Figure 13), as well as aromatics (not shown here).
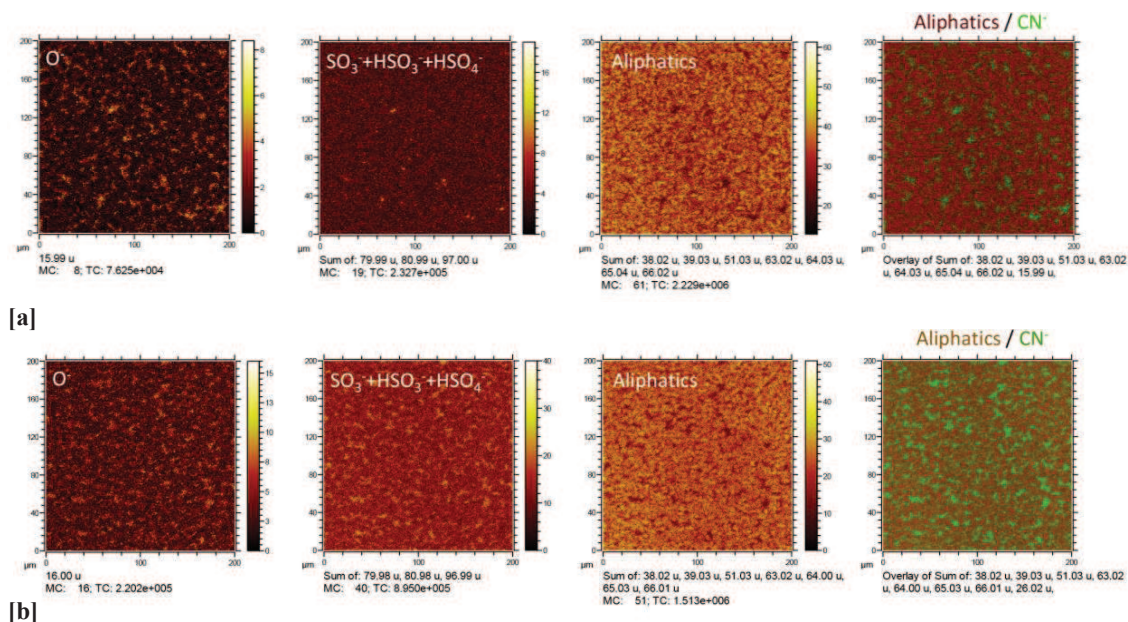
Figure 13: High-resolution TOF-SIMS images of selected negative fragment ions on the surface of bitumen C before [a] and after ageing [b]. The signal intensities in the images are given as the maximum number of ion counts per pixel (MC) and total ion counts in the entire image (TC).

4. Conclusions

In this work, the oxidative ageing mechanisms of three binders were investigated by FTIR, EPR and TOF SIMS. Binders were aged with modified thin-film oven test at a temperature of 50 °C. Consistent with previous studies the results from FTIR support the existence of two rate-determining oxidation phases, a fast- and a slow-rate and a rapid sulfoxide formation during the fast. For the examined binders this transition point was found to be between 2 and 5 days. Synchronous EPR measurements demonstrate that the overall amount of organic carbon-centred radicals evolves with the fast-rate phase. Taken together, the findings of the FTIR and TOF-SIMS spectrometry indicate that sulfoxide-, nitrogen- and oxygen-containing compounds, e.g. alcohols and/or carboxylic acids, are formed after the occurring fast- and slow-rate phases. An increase of aromatics and the accompanied decrease of aliphatics was only observed for the wax-containing binder.

Overall, the insights gained from this study may be particularly interesting for laying the groundwork for future research into the underlying oxidation mechanisms in bitumen. Future work could include more binder types or different ageing conditions. Of particular interest could be to investigate whether standardised accelerated ageing simulations would induce similar changes as observed in this study using a representative temperature.

Acknowledgements

16

References

[1]   J.S. Moulthrop, M. Massoud, The SHRP Materials Reference Library, Washington DC, 1993.

[2]   X. Lu, P. Sjövall, H. Soenen, Structural and chemical analysis of bitumen using time-of-flight secondary ion mass spectrometry (TOF-SIMS), Fuel. 199 (2017) 206–218. https://doi.org/10.1016/j.fuel.2017.02.090.

[3]   J.C. Petersen, R.E. Robertson, J.F. Branthaver, P.M. Harnsberger, J.J. Duvall, S.S. Kim, H.U. Bahia, R. Dongre, C.E. Antle, M.G. Sharma, Binder Characterization and Evaluation Volume 4 : Test M ethods, Washington DC, 1994.

[4]   J.C. Petersen, R. Glaser, Asphalt Oxidation Mechanisms and the Role of Oxidation Products on Age Hardening Revisited, Road Mater. Pavement Des. 12 (2011) 795–819. https://doi.org/10.1080/14680629.2011.9713895.

[5]   L.M. De Carvalho, C.S. Grassmann, C. Paulo, D. Bohrer, A.C. Fröhlich, C.K. Hoinacki, F.R. Adolfo, L.E. Claussen, M. Cravo, L.F.M. Leite, Distribution of sulfur compounds in Brazilian asphalt cements and its relationship to short-term and long-term aging processes, Constr. Build. Mater. 117 (2016) 72–79. https://doi.org/10.1016/j.conbuildmat.2016.04.111.

[6]   J.C. Petersen, A Review of the Fundamentals of Asphalt Oxidation (E-C140), Transp. Res. Rec. J. Transp. Res. Board. (2009). https://doi.org/10.17226/23002.

[7]   J. Knotnerus, Oxygen uptake by bitumen solutions as a potential measure of bitumen durability, Am. Chem. Soc. Div. Pet. Chem. 16 (1971) D37–D59.

[8]   T. Mill, The role of hydroaromatics in oxidative aging in asphalt, ACS Div. Fuel Chem. Prepr. 41 (1996) 1245–1248.

[9]   G. King, Oxycyclics : Understanding catalyzed oxidation mechanisms in bitumen and other petroleum products, Fuel Sci. Technol. Int. 11 (1993) 201–238. https://doi.org/10.1080/08843759308916063.

[10]   P. Herrington, B. James, T.F.P. Henning, Validation of a Bitumen Oxidation Rate Model, Transp. Res. Rec. J. Transp. Res. Board. 2632 (2017) 110–118. https://doi.org/10.3141/2632-12.

[11]   J. Petersen, P. Harnsberger, Asphalt Aging: Dual Oxidation Mechanism and Its Interrelationships with Asphalt Composition and Oxidative Age Hardening, Transp. Res. Rec. J. Transp. Res. Board. 1638 (1998) 47–55. https://doi.org/10.3141/1638-06.

[12]   P.R. Herrington, Diffusion and reaction of oxygen in bitumen films, Fuel. 94 (2012) 86–92. https://doi.org/10.1016/j.fuel.2011.12.021.

[13]   P.K. Das, R. Balieu, N. Kringos, B. Birgisson, On the oxidative ageing mechanism and its effect on asphalt mixtures morphology, Mater. Struct. 48 (2014) 3113–3127. https://doi.org/10.1617/s11527-014-0385-5.

[14]   B. Hofko, L. Porot, A.F. Cannone, L. Poulikakos, L. Huber, X. Lu, H. Grothe, K. Mollenhauer, FTIR spectral analysis of bituminous binders : reproducibility and impact of ageing temperature, Mater. Struct. 51 (2018). https://doi.org/10.1617/s11527-018-1170-7.

[15]   L.D. Poulikakos, C.F. A, D. Wang, L. Porot, B. Hofko, Impact of asphalt aging temperature on chemomechanics, RSC Adv. 9 (2019) 11602–11613. https://doi.org/10.1039/C9RA00645A.

[16]   S.-C. Huang, H. Di Benedetto, Advances in Asphalt Materials, 2015. https://doi.org/978-0-08-100269-8.

[17]   R. Tauste, Understanding the bitumen ageing phenomenon : A review, Constr. Build. Mater. 192 (2018) 593–609. https://doi.org/10.1016/j.conbuildmat.2018.10.169.

[18]   X. Lu, U. Isacsson, Effect of ageing on bitumen chemistry and rheology, Constr. Build. Mater. 16 (2002) 15–22. https://doi.org/10.1016/s0950-0618(01)00033-2.

[19]   A. Dony, L. Ziyani, I. Drouadaine, S. Pouget, S. Faucon-Dumont, D. Simard, V. Mouillet, J.E. Poirier, T. Gabet, L. Boulange, A. Nicolai, C. Gueit, 1, MURE National Project : FTIR spectroscopy study to assess ageing of asphalt mixtures, in: 6th Eurasphalt Eurobitume Congr., 2016. https://doi.org/dx.doi.org/10.14311/EE.2016.154.

[20]   F.J. Ortega, F.J. Navarro, M. Jasso, L. Zanzotto, Physicochemical softening of a bituminous binder by a reactive surfactant (dodecenyl succinic anhydride , DSA), Constr. Build. Mater. 222 (2019) 766–775. https://doi.org/10.1016/j.conbuildmat.2019.06.117.

378	[21]	J. Lamontagne, P. Dumas, V. Mouillet, J. Kister, Comparison by Fourier transform infrared (FTIR)
379		spectroscopy of different ageing techniques : application to road bitumens, Fuel. 80 (2001) 483–488.
380		https://doi.org/10.1016/S0016-2361(00)00121-6.
381	[22]	G. Tarsi, A. Varveri, C. Lantieri, A. Scarpas, C. Sangiorgi, Effects of Different Aging Methods on
382		Chemical and Rheological Properties of Bitumen, J. Mater. Civ. Eng. 30 (2018).
383		https://doi.org/10.1061/(asce)mt.1943-5533.0002206.
384	[23]	A. Vaitkus, A. Zofka, Evaluation of bitumen fractional composition depending on the crude oil type and
385		production technology, in: 9th Int. Conf. Environ. Eng., 2014.
386	[24]	P. Mikhailenko, H. Baaj, Comparison of Chemical and Microstructural Properties of Virgin and Reclaimed
387		Asphalt Pavement Binders and Their Saturate , Aromatic , Resin , and Asphaltene Fractions, Energy &
388		Fuels. 33 (2019) 2633–2640. https://doi.org/10.1021/acs.energyfuels.8b03414.
389	[25]	K. Zhao, Y. Wang, F. Li, Influence of ageing conditions on the chemical property changes of asphalt
390		binders, Road Mater. Pavement Des. (2019) 1–29. https://doi.org/10.1080/14680629.2019.1637771.
391	[26]	P. Mikhailenko, C. Kou, H. Baaj, L. Poulikakos, A. Cannone-falchetto, J. Besamusca, B. Hofko,
392		Comparison of ESEM and physical properties of virgin and laboratory aged asphalt binders, Fuel. 235
393		(2019) 627–638. https://doi.org/10.1016/j.fuel.2018.08.052.
394	[27]	D. Grossegger, Microstructural aging of bitumen Microstructural aging of bitumen, in: 6th Eurasphalt
395		Eurobitume Congr., 2016. https://doi.org/10.14311/EE.2016.135.
396	[28]	X. Lu, P. Sjövall, H. Soenen, M. Andersson, Microstructures of bitumen observed by environmental
397		scanning electron microscopy (ESEM) and chemical analysis using time-of- flight secondary ion mass
398		spectrometry (TOF-SIMS), Fuel. 229 (2018) 198–208. https://doi.org/10.1016/j.fuel.2018.05.036.
399	[29]	J.P. Aguiar-moya, J. Salazar-delgado, A. García, A. Baldi-, V. Bonilla-mora, L.G. Loría-salazar, J. Salazar-
400		delgado, A. García, A. Baldi-, Effect of ageing on micromechanical properties of bitumen by means of
401		atomic force microscopy, Road Mater. Pavement Des. 18 (2017) 203–215.
402		https://doi.org/10.1080/14680629.2017.1304249.
403	[30]	Y. Cui, C.J. Glover, J. Braziunas, H. Sivilevicius, Further exploration of the pavement oxidation model
404		Diffusion-reaction balance in asphalt, Constr. Build. Mater. 161 (2018) 132–140.
405		https://doi.org/10.1016/j.conbuildmat.2017.11.095.
406	[31]	R. Karlsson, U. Isacsson, Laboratory studies of diffusion in bitumen using markers, J. Mater. Sci. 38 (2003)
407		2835–2844. https://doi.org/10.1023/A:1024476217060.
408	[32]	R. Han, X. Jin, C.J. Glover, Petroleum Science and Technology Oxygen Diffusivity in Asphalts and
409		Mastics, Pet. Sci. Technol. (2013) 37–41. https://doi.org/10.1080/10916466.2011.559506.
410	[33]	A. Stoll , S.; Schweiger, EasySpin, a comprehensive software package for spectral simulation and analysis
411		in EPR, J. Magn. Reson. 178 (2006) 42–55. https://doi.org/https://doi.org/10.1016/j.jmr.2005.08.013.
412	[34]	M. Espinosa; P.A. Camper; R. Salcedo, Electron Spin Resonance and Electronic Structure of
413		Vanadyl−Porphyrin in Heavy Crude Oils, Inorg. Chem. 40 (2001) 4543–4549.
414		https://doi.org/https://doi.org/10.1021/ic000160b.
415	[35]	L.G. Gilinskaya, EPR spectra of V(IV) complexes and the structure of oil porphyrins, J. Struct. Chem. 49
416		(2008) 245–254. https://doi.org/10.1007/s10947-008-0120-6.
417	[36]	N.S. Ramachandran, Vasanth; van Tol, Johan; McKenna, Amy M.; Rodgers, Ryan P. ; Alan G. Marshall,
418		Ryan P. ; Dalal, High Field Electron Paramagnetic Resonance Characterization of Electronic and Structural
419		Environments for Paramagnetic Metal Ions and Organic Free Radicals in Deepwater Horizon Oil Spill Tar
420		Balls, Anal. Chem. 87 (2015) 2306–2313. https://doi.org/10.1021/ac504080g.
421	[37]	V. Thiel, P. Sjövall, Time-of-Flight Secondary Ion Mass Spectrometry (TOF-SIMS): Principles and
422		Practice in the Biogeosciences, in: Princ. Pract. Anal. Tech. Geosci., Royal Society of Chemistry, 2015:
423		pp. 122–170.
424	[38]	J.H. Tannous, A. De Klerk, Quantification of the Free Radical Content of Oilsands Bitumen Fractions,
425		Energy & Fuels. 33 (2019) 7083–7093. https://doi.org/10.1021/acs.energyfuels.9b01115.
426	[39]	M.F. Libert, I. Walczak, Effect of radio-oxidative ageing and pH on the release of soluble organic matter
427		from bitumen, in: Int. Conf. Sci. Res. Back-End Fuel Cycle 21. Century, France, 2000: pp. 1–4.

18

428   [40]   G. Boczkaj, A. Przyjazny, M. Kamin, Characteristics of volatile organic compounds emission profiles from
429   hot road bitumens, Chemosphere. 107 (2014) 23–30. https://doi.org/10.1016/j.chemosphere.2014.02.070.
430   [41]   I.-H. Wang, J.L. Boucher, R.A. Romine, R.D. Rowlett, G.-D. Lei, Oxidation chemistry in asphalt, Fuel Sci.
431   Technol. Int. 11 (1993) 1–28. https://doi.org/http://dx.doi.org/10.1080/08843759308916056.